ACS APPLIED MATERIALS & INTERFACES

Research Article

www.acsami.org

Mesoporous Submicrometer TiO_2 Hollow Spheres As Scatterers in Dye-Sensitized Solar Cells

Shabnam Dadgostar,[†] Fariba Tajabadi,*[,‡] and Nima Taghavinia*[,‡,§]

[†]Department of Physics, Tarbiat Modarres University, Gisha Bridge, Tehran 1411717751, Iran

[‡]Physics Department, Sharif University of Technology, Azadi Avenue, Tehran 14588, Iran

[§]Institute for Nanoscience and Nanotechnology, Sharif University of Technology, Tehran 14588, Iran

Supporting Information

ABSTRACT: Hierarchical submicrometer TiO_2 hollow spheres with outer diameter of 300−700 nm and shell thickness of 200 nm are synthesized by liquid phase deposition of TiO_2 over carbon microspheres as sacrificial templates. The final TiO_2 hollow spheres are applied as a scattering layer on top of a transparent nanocrystalline TiO_2 film, serving as the photoanode of a dye-sensitized solar cell (DSC). In addition to efficient light scattering, the mesoporous structure of TiO_2 hollow spheres provides a high surface area, 74 m^2/g, which allows for higher dye loading. This dual functioning suggests that TiO_2 hollow spheres may be good replacements for conventional TiO_2 spheres as scatterers in DSCs. A high efficiency of 8.3% is achieved with TiO_2 hollow spheres, compared with 6.0% for the electrode with 400 nm spherical TiO_2 scatterers, at identical conditions.

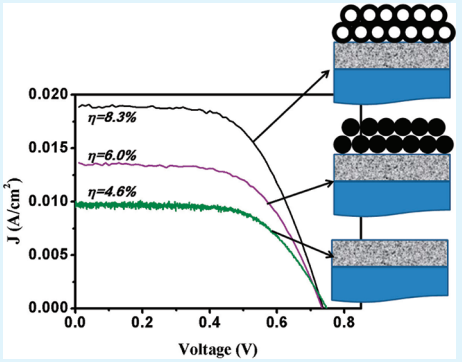

KEYWORDS: *dye-sensitized solar cell, TiO_2 hollow sphere, scattering layer*

1. INTRODUCTION

During the past two decades, dye-sensitized solar cells (DSCs) have been intensively investigated as a promising alternative for the conventional silicon-based solar cells because of their potentially low production cost and facile technology.[1] Much effort has been made toward improving the performance of DSCs by optimizing photosensitizers, photoanode, redox electrolyte, and counter electrode.[2−5] Among these, the structure and morphology of photoanode plays a critical role in determining the final light to electricity conversion efficiency. Generally, high specific surface area, fast electron transport, and effective light scattering are desirable properties for a well-performing photoanode. In highly efficient DSCs, the photoelectrode is normally made of anatase TiO_2 nanocrystals of ∼20 nm in diameter, to ensure a large internal surface area for loading large amounts of dye molecules. Because such a film is well transparent, resulting in the transmittance of long wavelength (red) part of the incident light without exciting dye molecules, a second layer of TiO_2 anatase particles of ∼400 nm in diameter is often used to scatter back the transmitted light, in order to enhance light harvesting.[6] However, because of low surface area for dye adsorbing the second overlayer only serves to enhance light scattering, with small contribution in light absorption. This is not, in principle, desirable as the large TiO_2 particles increase the total volume of the semiconductor photoanode, while contribute little in electron injection. This effectively reduces the electron concentration and quasi Fermi level. It is, therefore, useful to increase light absorption by scattering effects while maintaining a high specific surface area of the photoanode films for efficient dye adsorption. Recently, increased attention has been paid to the utilization of nanoporous and/or mesoporous TiO_2 submicrometer microspheres as photoanodes in DSCs, and high energy conversion efficiencies (7.2−8.4%) have been obtained.[7]

Here we report the synthesis of hierarchical submicrometer TiO_2 hollow spheres (HS) by using carboxylate-rich carbon microspheres (CMS) as template. CMSs are synthesized by a facile and environmentally friendly route. The produced CMSs show a rough surface with high capacity for metal ion adsorption.[8] Liquid phase deposition method was used for deposition of TiO_2 on carbon microspheres. A 3D network of hierarchical submicrometer HSs were formed after removing the carbon template at high temperature, exhibiting high specific surface area as well as good light scattering property. Although similar hierarchical TiO_2 particles have been reported previously, our synthesis allowed the adhesion of the TiO_2 mesoporous microspheres with each other by 3D necking during the film formation, thus significantly enhancing the intermicrosphere connectivity, facilitating electron transport. An overall energy conversion up to 8.3% has been attained for the composition of TiO_2 nanoparticles and HSs, which is about 1.4 fold more than the efficiency of the composition of TiO_2 nanoparticles and 400 nm TiO_2 filled spheres (FS).

Received: February 24, 2012
Accepted: May 19, 2012
Published: May 19, 2012

2. EXPERIMENTAL SECTION

CMSs, with a high degree of surface functional groups, were prepared in an aqueous solution of glucose (0.5M) and acrylic acid (5 mM). The solution was hydrothermally treated in a Teflon lined autoclave for 16 h at 190 °C. After cooling naturally to room temperature the black precipitate was washed several times by water and ethanol and dried in oven at 80 °C.

HSs were prepared by liquid phase deposition of TiO_2 on the CMSs substrates. A solution of $(NH_4)_2TiF_6$ (0.05M) and H_3BO_3 (0.15 M) was prepared and added to 0.1 g of carbon spheres. The mixture was sonicated for 10 min, and then heated at 50 °C for 24 h. The black precipitate was filtrated and dried at 80 °C for 1 h and finally heated at 490 °C to remove the carbon template. A white TiO_2 powder is produced. As illustrated schematically in Scheme 1, the process is expected to result in hollow spheres of TiO_2. HSs were used to make a screen printing paste to study them as the scattering layer in DSCs.

Scheme 1. Scheme of Three Phases of TiO_2 HS Production, Illustrating the Growth of a Nanostructured Film over a CMS Template, And Thermal Removal of the Template

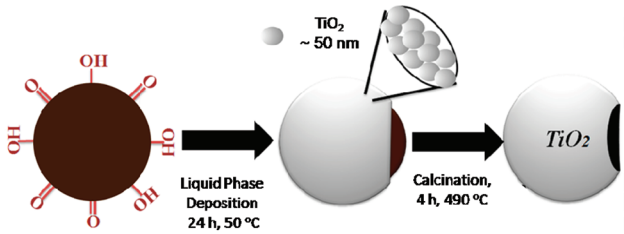

TiO_2 photoelectrodes for DSCs were created by Doctor Blade deposition of a transparent nanocrystalline TiO_2 film of 8 μm thickness, consisting of ~20 nm TiO_2 nanocrystals. Three different photoanode structures were studied: a single transparent film without any scattering layer (T), the transparent film overcoated with a 6 μm conventional scattering layer of ~400 nm filled spheres of anatase TiO_2 (T-FS), and the transparent film overcoated with a 6 μm HS layer (T-HS). The pasted films were heat treated at 490 °C for calcination and sintering, and $TiCl_4$ was treated in a solution of 40 mM for 30 min. The mesoporous films were dye loaded in a 0.3 mM N719 (B2, Dyesol) dye solution. Counter electrodes were prepared by thermal deposition of 0.3 mM H_2PtCl_6 solution in ethanol, spread on FTO. 30 μm Surlyn (Dyesol) spacers were used to seal the cells. The cells were filled with an electrolyte composed of 0.6 M 1-butyl-3-methylimidazolium iodide (BMII), 0.1 M guanidiniumthiocyanate (GuSCN), 0.03 M I_2, and 0.5 M 4-tertbutylpyridine (Aldrich) in acetonitrile/valeronitrile (85:15, vol%).

The morphology of CMSs and HSs were observed by field emission scanning electron microscopy (Hitachi 4160). *I*–*V* curves of the DSCs have been measured under AM1.5 simulated solar light (100 mW/cm^2) (Luzchem Solar). Incident photon to current conversion efficiency (IPCE) spectra were recorded on a Jarrell Ash monochromator, using a 100 W halogen lamp and a calibrated photodiode (Thorlabs). Diffuse reflectance and transmittance spectra of the films have been collected by Avaspec2048-TEC UV–vis-NIR spectrophotometer using an integrating sphere. Dye loading on mesoporous TiO_2 films was measured by desorption of dye through soaking dye-sensitized TiO_2 films in 0.1 M NaOH aqueous solution, and measuring the concentration of desorbed dyes by absorption measurement.

3. RESULTS AND DISCUSSION

Figure 1 shows the scanning electron microscopy (SEM) images of coated and uncoated CMS particles, as well as CMS omitted HSs. Obviously, CMSs have spherical morphology in size range between 400 and 1000 nm. It has been demonstrated that the surface is rich with functional groups such as carboxylic groups,[8] which provides a good chemistry for liquid phase deposition of TiO_2, as the surface chemical activity is crucial for successful sol–gel nucleation and growth on the surface.[9] In the presence of CMSs, hydrolyzed Ti species condense on the surface of CMSs at the functional groups, and the process continues on the basis of a heterogeneous nucleation and growth scheme.[10] The deposited layers are apparently porous (Figure 1b,c). CMSs are finally thermally removed and TiO_2 HSs are formed (see Scheme 1). Particles are spheres in the size range of 300–700 nm with shell thickness of 200 nm. This is a smaller size compared to the size of original CMSs, and shows the TiO_2 shell shrinks during the carbon removal. The size range of 300–700 nm is ideal for light scattering in the visible and near-infrared region.[11] HSs show a mesoporous structure of aggregated particles, with SEM size of 30–50 nm. BET surface area of HSs was measured at 74 m^{2}g^{-1} with a distribution of pore sizes below 20 nm (see the Supporting Information). This is a remarkable specific surface area and corresponds to spherical grains of about 20 nm. HSs can, therefore, contribute in dye adsorption and enhance the light

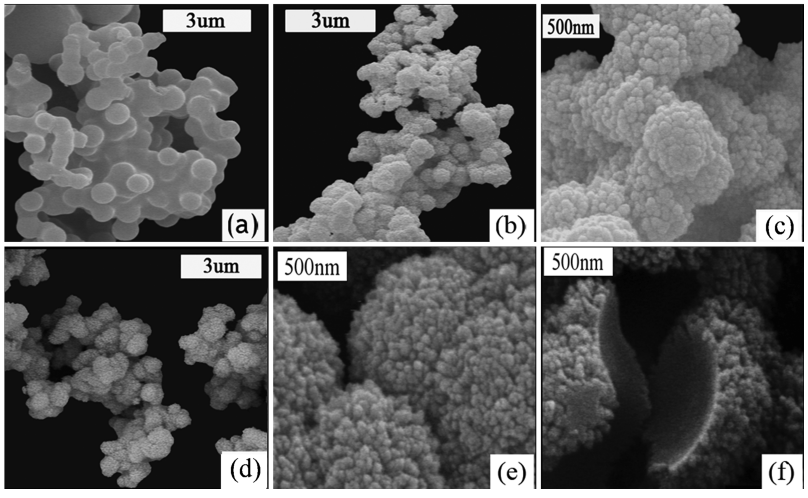

Figure 1. SEM images of (a) carbon micro spheres (CMSs), (b,c) TiO_2-coated CMSs before thermal removal of carbon, (d–f) HSs after removal of carbon template.

harvesting of the cells. The pore size and BET surface area of the HSs can be controlled by the LPD conditions and using differently prepared CMS templates (see the Supporting Information). Nevertheless, their optical properties are almost identical, and therefore, here we have adopted the structure with the highest BET surface area.

The photovoltaic performance of the cells with photoanode structures T, T-FS and T-HS are displayed in Table 1 and

Table 1. Photovoltaic Properties of the DSCs Prepared with and without the Scattering Layers[a]

sample	d_T (μm)	d_s (μm)	N_{dye} (cm^{-2})	V_{oc} (V)	J_{sc}(mA cm^{-2})	η (%)	FF(%)
T	8	0	5.1×10^{16}	0.76	9.7	4.6	60.7
T-FS	8	6	5.6×10^{16}	0.73	13.6	6.0	60.7
T-HS	8	6	7.2×10^{16}	0.74	19.0	8.3	59.7

[a] d_T, d_s, and N_{dye} denote the thickness of transparent film, thickness of scattering layer, and number of adsorbed dye molecules, respectively.

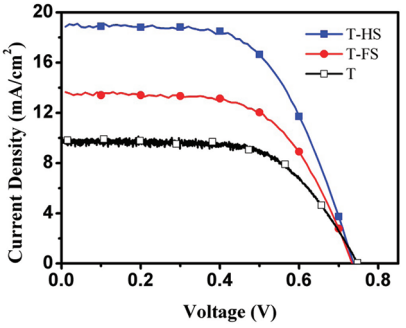

Figure 2. $I-V$ curves of DSCs with a photoanode of a single transparent film (T) without a scattering layer, and with filled sphere (FS) and hollow sphere (HS) scattering layers.

Figure 2. As shown in Table 1, the dye loading on T-FS cell, comprising the conventional 400 nm filled sphere scatterers, is about 10% more than the single transparent film (T), while this increase is about 40% for the T-HS cell. This is considerable, as with the same thickness and scattering functionality, the loading of the absorbing dyes is remarkably better for T-HS cells.

The photovoltaic performance also differs drastically. The improvement is mainly in the current density of the cells, where T-HS cells show J_{sc} up to 19.0 mA/cm^2, compared to 13.6 and 9.7 mA/cm^2 for T-FS and T cells. This is an evidence for better light harvesting through dye loading and light scattering by hollow spheres. The Open circuit voltage (V_{oc}) is not much dependent on the scattering layer. V_{oc} decreases from 0.76 V in no-scatterer cell (T) to 0.73 and 0.74 V for filled (T-FS) and hollow sphere (T-HS) scatterer cells. Higher V_{oc} of the T cell is a result of lower surface area of the mesoporous electrode, that is, less recombination of electrons with the electrolyte. For T-HS, V_{oc} is slightly higher than T-FS cell; i.e. the electron concentration is higher in T-HS electrodes. Despite larger surface area provided by HSs, which favor higher recombination and lower V_{oc}, more injected electrons in a smaller volume of TiO_2 produces larger electron concentration in the electrode. Higher electron injection is caused by larger dye loading by HSs. On the other hand, hollow spheres possess smaller volume compared to filled spheres, which causes larger electron concentration for a certain number of injected electrons. The total volume of the semiconductor electrode is an important parameter that is usually neglected.

A major role of the scattering layer is light back reflection and increase of light path inside the mesoporous electrode. The diffuse reflectance and transmittance spectra for dye loaded T, T-FS, and T-HS electrodes are shown in Figure 3. The data

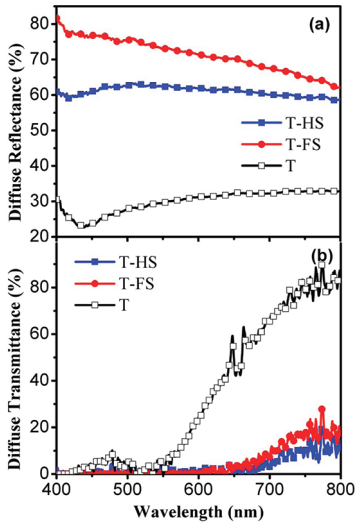

Figure 3. (a) Diffuse reflectance and (b) diffuse transmittance of dye-loaded photoanodes of T, T-FS, and T-HS.

clearly shows that both FS and HS are effective in enhancing the light absorption, in particular in wavelengths larger than 550 nm. Diffuse transmittance spectra demonstrate that a small portion of light in 700−800 nm range can pass through the electrode without absorption.

Although both FS and HS scattering layers make a considerable enhancement in the diffuse reflectivity, there is a distinction between them, in that FS shows a higher diffuse reflectance, especially at short wavelengths. The two curves approach to each other at 800 nm, where there is no dye absorption. This reveals that FS and HS layers possess similar scattering power, whereas in case of HS, higher light absorption at shorter wavelengths causes lower back reflection of the incident light.

The incident-photon-to-current conversion efficiency (IPCE) spectra (Figure 4) provide more evidence on the scattering effect. T-FS and T-HS cells show higher IPCE than that of T cell over the entire wavelength region, which is in agreement with the observed higher J_{sc} due to light scattering. The main enhancement caused by the scattering layers occurs

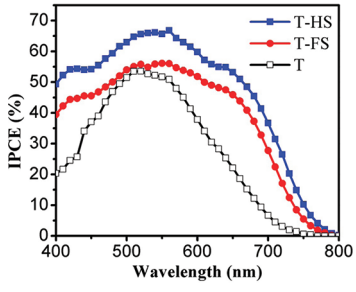

Figure 4. Incident photon to current conversion efficiency for T, T-FS, and T-HS cells.

in wavelengths with small dye absorption, in particular in the long wavelength side. T-HS cells show superior photon to current conversion efficiency, which results from higher dye loading, as well as efficient light scattering.

Figure 5 shows the Nyquist plots under the open circuit condition for T, T-FS, and T-HS cells. In general, three

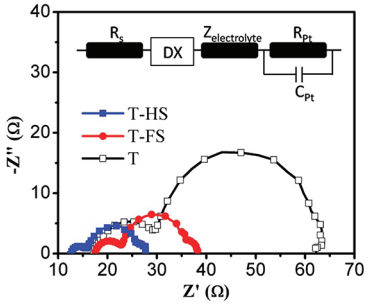

Figure 5. EIS curves for T, T-FS, and T-Hs cells. The inset shows the circuit model used to obtain the values of circuit elements. DX is a distributed element, as defined by Bisquert.

semicircles extending from total resistance can be recognized and fitted according to an equivalent circuit. The semicircle in the high frequency region (1×10^5 to 1×10^2 Hz) represents the impedance corresponding to charge transfer at the counter electrode (R_{pt}), while those in intermediate frequencies (1×10^2 to 1×10 Hz) give information on the impedance at the TiO_2/electrolyte interface related to the charge transport/recombination, and the low-frequency region (10−0.1 Hz) represents the finite diffusion of the electrolyte, respectively. A significant difference can be seen in the second semicircle of the impedance spectra that represents the resistance component at the TiO_2/electrolyte interface. The fitted data using Bisquert model are represented in Table 2. Both recombination

Table 2. Cell Parameters Obtained by Fitting the EIS Curves with the Mode[a]

sample	R_{rec} (Ω)	R_t (Ω)	τ_n(ms)
T	30	10	25
T-FS	15	6	12.5
T-HS	11	2	10

[a] R_{rec}, R_t, and τ_n denote the recombination resistance, transport resistance, and electron lifetime, respectively.

resistance and transport resistance show a decreasing trend as T-HS < T-FS < T.[12] Two factors can be invoked to explain this trend: light absorption and photoanode surface area. Increasing photoanode surface causes more recombination probability those results in lower recombination resistance in TiO_2/electrolyte interface.

Therefore, it is expected that addition of scattering layer to the absorbing film decreases recombination resistance. On the other hand, presence of scattering layer increases light absorption thus more photoelectrons are generated and injected into the photoanode, resulting in higher electron density and higher conductivity as seen in Table 2.

4. CONCLUSION

The use of TiO_2 HSs as scattering layer in DSCs apparently offers advantages over the conventional 400 nm TiO_2 spheres. HSs can scatter light, while maintaining considerable dye adsorption capacity. The scattering power of HSs is lower than FSs, as depicted in the reflectance spectra; however, this is overcompensated by the higher light absorption inside the HS layer. In principle, the most optimized semiconductor photoanode structure is one having sufficient absorption and scattering property, with lowest volume of semiconductor photoanode. This results in higher electron density by the injected electrons. This suggests that structures such as HSs and TiO_2 nanoparticle beads are superior.[7] Compared to TiO_2 nanoparticle beads, which also show both scattering and absorption property, hollow spheres possess an internal interface that is expected to enhance the scattering of light.

■ ASSOCIATED CONTENT

Supporting Information

Morphology of carbon microspheres and TiO_2 hollow spheres synthesized with alternative synthesis conditions, BET adsorption/desorption data, and PV performance of cells with thinner transparent layer. This material is available free of charge via the Internet at http://pubs.acs.org.

■ AUTHOR INFORMATION

Corresponding Author

*E-mail: tajabadi@ncl.sharif.edu (F.T); taghavinia@sharif.edu (N.T.).

Notes

The authors declare no competing financial interest.

■ REFERENCES

(1) O'Regan, B.; Gratzel, M. *Nature* **1991**, *353*, 737.
(2) Robertson, N. *Angew. Chem., Int. Ed.* **2006**, *45*, 2338. Gratzel, M. *Acc. Chem. Res.* **2009**, *42*, 1788. Mishra, A.; Fischer, M. K. R.; Bauerle, P. *Angew. Chem., Int. Ed.* **2009**, *48*, 2474. Hagfeldt, A.; Boschloo, G.; Sun, L.; Kloo., L.; Pettersson, H. *Chem. Rev.* **2011**, *110*, 6595.
(3) Luo, Y.; Li., D.; Meng, Q. *Adv. Mater.* **2009**, *21*, 1. Zhang, Q.; Cao, G. *J. Mater. Chem.* **2011**, *21*, 6769. Jose, R.; Thavasi, V.; Ramakrishna, S. *J. Am. Ceram. Soc.* **2009**, *92*, 289. Zhang, Q.; Dandeneau, C. S.; Zhou., X.; Cao, G. *Adv. Mater.* **2009**, *21*, 1.
(4) Boschloo., G.; Hagfeldt, A. *Acc. Chem. Res.* **2009**, *42*, 1819. Wu, J.; Lan, J.; Hao, S.; Li, P.; Lin, J.; Huang, M.; Fang., L.; Huang, Y. *Pure Appl. Chem.* **2008**, *80*, 2241.
(5) Murakami, T.; Gratzel, M. *Inorg. Chim. Acta* **2008**, *361*, 572. Hagfeldt, A.; Boschloo, G.; Sun, L.; Kloo, L.; Pettersson, H. *Chem. Rev.* **2011**, *110*, 6595. Luo, Y.; Li, D.; Meng, M. *Adv. Mater.* **2009**, *21*, 1.
(6) Wang, P.; Zakeeruddin, S. M.; Comte, P.; Charvet, R.; Humphry-Baker, R.; Gratzel, M. *J. Phys. Chem. B* **2003**, *107*, 14336. Gao, F.; Wang, Y.; Shi, D.; Zhang, J.; Wang, M. K.; Jing, X. Y.; Humphry-Baker, R.; Wang, P.; Zakeeruddin., S. M.; Gratzel, M. *J. Am. Chem. Soc.* **2008**, *130*, 10720. Ito, S.; Murakami, T. N.; Comte, P.; Liska, P.; Grätzel, C.; Nazeeruddin, M. K.; Grätzel, M. *Thin Solid Films* **2008**, *516*, 4613.
(7) Kim, Y. J.; Lee, M. H.; Kim, H. J.; Lim, G.; Choi, Y. S.; Park, N. G.; Kim, K.; Lee, W. I. *Adv. Mater.* **2009**, *21*, 3668. Chen, D.; Huang, F.; Cheng, Y. B.; Caruso, R. A. *Adv. Mater.* **2009**, *21*, 2206. Yang, W. G.; Wan, F. R.; Chen, Q. W.; Li, J. J.; Xu, D. S. J. *Mater.Chem.* **2010**, *20*, 2870. Sauvage, F.; Chen, D.; Comte, P.; Huang, F.; Heiniger, L. P.; Cheng, Y. B.; Caruso, R. A; Graetzel, M. *ACS Nano* **2010**, *4*, 4420. Shao, W.; Gu, F.; Li., C.; Lu, M. *Inorg. Chem.* **2010**, *49*, 5453. Yan, K.; Qiu, Y.; Chen, W.; Zhang, M.; Yang, S. *Energy Environ. Sci.* **2011**, *4*, 2168. Wang, H. E.; Zheng, L. X.; Liu, C. P.; Liu, Y. K.; Luan, C. Y.; Cheng, H.; Li, Y. Y.; Martinu, L.; Zapien, J. A.; Bello, I. *J. Phys. Chem. C* **2011**, *115*, 10419.
(8) Cakan, R. D.; Baccile, N.; Antonietti, M; Titirici, M. M. *Chem. Mater.* **2009**, *21*, 484.
(9) Pourmand, M.; Taghavinia, N. *Mater. Chem. Phys.* **2008**, *107*, 449.
(10) Shin, M.; Agarwal, DeGuire., M. R.; Heuer, A. H. *Acta Mater.* **1998**, *46*, 801.

(11) Ferber, J.; Luther, J. *Sol. Energy Mater. Sol. Cells* **1998**, *54*, 265.
(12) Bisquert, J.; Gratzel, M.; Wang, Q.; Fabregat-Santiago, F . *J. Phys. Chem. B* **2006**, *110*, 11284.